Optomechanical Frequency Comb Based on Multiple Nonlinear Dynamics

Yu Wang,[*] Mai Zhang,[*] Zhen Shen,[†] Guan-Ting Xu, Rui Niu, Fang-Wen Sun, Guang-Can Guo, and Chun-Hua Dong[‡]

CAS Key Laboratory of Quantum Information, University of Science and Technology of China, Hefei, Anhui 230026, China;
CAS Center For Excellence in Quantum Information and Quantum Physics, University of Science and Technology of China, Hefei, Anhui 230088, China;
and Hefei National Laboratory, University of Science and Technology of China, Hefei, Anhui 230088, China

(Received 25 October 2023; accepted 25 March 2024; published 19 April 2024; corrected 8 May 2024)

Phonon-based frequency combs that can be generated in the optical and microwave frequency domains have attracted much attention due to the small repetition rates and the simple setup. Here, we experimentally demonstrate a new type of phonon-based frequency comb in a silicon optomechanical crystal cavity including both a breathing mechanical mode (∼GHz) and flexural mechanical modes (tens of MHz). We observe strong mode competition between two approximate flexural mechanical modes, i.e., 77.19 and 90.17 MHz, resulting in only one preponderant lasing, while maintaining the lasing of the breathing mechanical mode. These simultaneous observations of two-mode phonon lasing state and significant mode competition are counterintuitive. We have formulated comprehensive theories to elucidate this phenomenon in response to this intriguing outcome. In particular, the self-pulse induced by the free carrier dispersion and thermo-optic effects interacts with two approximate flexural mechanical modes, resulting in the repetition rate of the comb frequency-locked to exact fractions of one of the flexural mechanical modes and the mode hopping between them. This phonon-based frequency comb has at least 260 comblines and a repetition rate as low as a simple fraction of the flexural mechanical frequency. Our demonstration offers an alternative optomechanical frequency comb for sensing, timing, and metrology applications.

DOI: 10.1103/PhysRevLett.132.163603

Introduction.—Frequency combs consist of a series of equally spaced, discrete narrow spectral lines and have been realized in the optical frequency combs (OFCs) [1–6] and the microwave frequency combs (MFCs) [7,8]. OFCs have received widespread attention in the past quarter century and been widely used in frequency metrology, atomic clocks, optical ranging, optical communication, astronomical spectrograph calibration, low-noise microwave, and quantum entanglement states [2–4,9–16]. To support these wide range of applications, OFCs that enable coverage at different spectral regions and varying frequency resolutions have been demanded. Meanwhile, the development of systems that offer reduced size, weight, and power (SWaP) remains an important objective for future OFCs [17]. However, for integrated optical microcombs [4,5], which are designed to be more SWaP friendly, it is still a challenge to achieve a repetition rate < 1 GHz due to the requirement for a large cavity with high Q [18,19]. Additionally, MFCs can be employed in multichannel microwave radars, arbitrary waveform generations, and Doppler reflectometry [20–22]. However, the conventional MFC demonstrations [7,8] are associated with complicated setups.

Mechanical degrees of freedom can be observed across a wide frequency range spanning from the Hz to THz [23–28], and can be found in various quantum regimes as an interface candidate for quantum networks [29–31]. Moreover, phonons and photons, both being bosons, exhibit striking similarities [32], and the parametric coupling between them can be expressed as a strong third-order nonlinear effect [33]. All of these spark interest in studying phonon-based frequency combs [19,33–37], as they hold potential for integrated optical microcombs with a repetition rate < 1 GHz, for MFCs with simple setups.

In recent years, based on the theory of Fermi-Pasta-Ulam-Tsingou chain [38], a direct analog for OFCs in the phononic domain has been demonstrated [34,35]. Using the nonlinearity arising from the parametric coupling between phonons and photons to simulate the Kerr nonlinear effect [4,39], frequency combs mediated by single or multiple mechanical mode lasing have been demonstrated in optomechanical systems [19,36,37,40]. However, the phenomenon of multimode competition and coexistence of multimode phonon lasing (MPL) has been observed separately in individually designed experiments [41,42], yet a comprehensive explanation and verification are still lacking.

In this Letter, we experimentally show a new kind of optomechanical frequency combs (OMFCs) based on MPL

and self-pulse process [43,44]. Without any additional manipulation, the two-mode phonon lasing state generates, i.e., both 5.26 GHz breathing mechanical mode and 90.17 MHz flexural mechanical mode undergo self-sustained oscillation. Interestingly, another approximate flexural mechanical mode, i.e., 77.19 MHz, is suppressed during the comb generation. These simultaneous observations of the two-mode phonon lasing state and significant mode competition are counterintuitive. We have developed comprehensive theories to elucidate this intriguing phenomenon in detail. In particular, the self-pulse (SP) induced by the free carrier dispersion and thermo-optic effects interacts with two approximate flexural mechanical modes, leading to the repetition rate of the comb being frequency locked to exact fractions of one flexural mechanical mode, and the mode hopping between two flexural mechanical modes. Through the cascaded four-wave mixing of the optical sidebands modulated by these MPL and frequency-locked SP, the OMFCs exhibit at least 260 combines and a repetition rate as low as a simple fraction of the flexural mechanical frequency. The participation of multiple nonlinear dynamics provides an abundant platform to generate the optomechanical frequency combs with the low repetition rate.

Multimode silicon optomechanical system.—The optomechanical crystal (OMC) cavity is fabricated from a silicon-on-insulator (SOI) wafer [28], as shown in Figs. 1(a)–1(b). Our device exhibits an optical cavity resonance at wavelength $\lambda_0 = 1532.785$ nm with total damping rate $\kappa = 885$ MHz, corresponding to Q factor of 2.2×10^5, as shown in Fig. 1(c). Additionally, the characterization of mechanical modes can be extracted from the power spectrum, as shown in Fig. 1(d). Two typical in-plane flexural mechanical modes ($m_{1,2}$) with lower frequency and a "breathing" mode (m_3) around 5 GHz are observed. The frequencies of mechanical modes are $\omega_1/2\pi = 77.19$ MHz, $\omega_2/2\pi = 90.17$ MHz, and $\omega_3/2\pi = 5.259$ GHz with damping rate $\gamma_1/2\pi = 7.63$, $\gamma_2/2\pi = 17.29$, and $\gamma_3/2\pi = 43.6$ kHz, respectively. The single-photon optomechanical coupling rates $g_1/2\pi = 47.9$, $g_2/2\pi = 76.5$, and $g_3/2\pi = 800$ kHz which originate from a combination of radiation pressure and photostriction, are calibrated from the measurements based on frequency modulation technique [45] and optomechanical induce transparency [46,47] technique

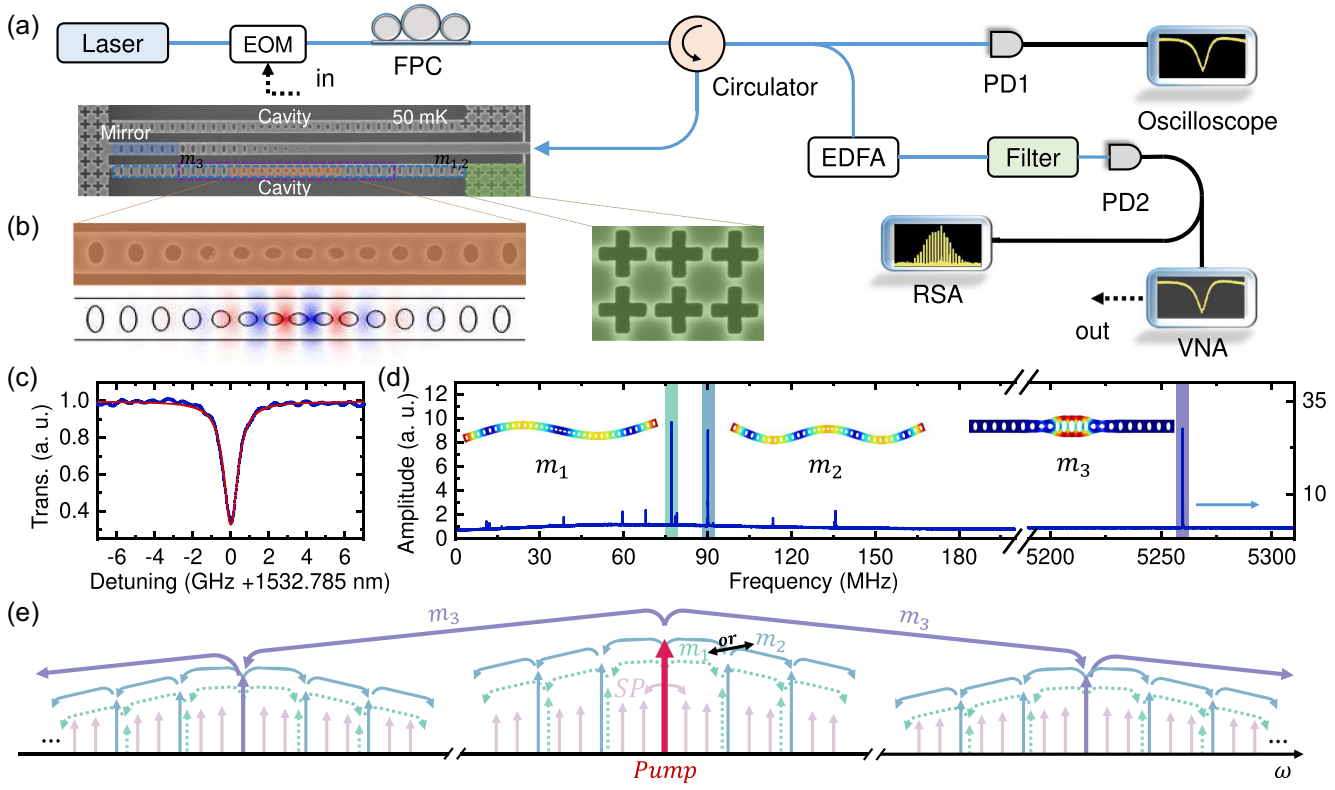

FIG. 1. (a) Schematic of the setup. The SEM image shows the device consisting of two nanobeam microcavities and a tapered waveguide with an OMC mirror. Electro-optic modulator (EOM); fiber polarization controller (FPC); photodetector (PD); erbiumdoped fiber amplifier (EDFA); realtime spectrum analyzer (RSA); vector network analyzer (VNA). (b) The expanded details of the device in (a). The orange and green area show a defective cavity and the 5 GHz phonon shielding structure, respectively. The bottom panel is the simulated electric field of the optical mode in the OMC cavity. (c)–(d) The transmission of optical mode and the power spectrum of mechanical modes in the OMC cavity. The insets show the in-plane flexural modes ($m_{1,2}$), and the breathing mode (m_3), respectively. (e) Schematic of OMFC originating from the nonlinear interactions between photons, multiple modes phonons, and self-pulse (SP).

using a VNA (see the Supplemental Material for more details [48]).

Optomechanical frequency combs.—Figure 1(e) depicts the schematic of the cascade mixing processes when driven by a strong pump laser. Here, the mechanical mode m_3 with greater g_3 is first excited to the lasing state, resulting in a series of optical sidebands with frequency ω_3. As we know, the multiple mechanical modes with similar parameters, especially frequency, cannot all be optomechanically driven to self-sustained oscillation state [41]. However, the significant frequency difference between mode m_3 and m_2 (or m_1) induces a weaker gain suppression from m_3 to other modes. Meanwhile, there will be intense competition among mechanical modes with similar parameters, such as m_1 and m_2. Consequently, the lasing state of the mechanical mode m_2 (or m_1) modulates light with frequency ω_2 (or ω_1), producing a series of optical sidebands around the pump and the sideband light generated by the mode m_3. In addition, when the SP was excited and coherently coupled with the mode m_2 (or m_1) in the system, more comb lines with denser frequency spacing would be generated. With assistance of SP, the lasing state between the modes m_1 and m_2 can be switched. These unique features of SP enhance the richness and tunability of our OMFC (see Supplemental Material for more details [48]).

Figure 2 illustrates the typical OMFCs when the pump laser scanned across the optical mode. The multimode oscillation lasing state of mechanical modes m_2 and m_3 could be observed at the beginning, as shown in Fig. 2(a). In this state, over 150 comb lines are observed within 60 dB power variation in the frequency range from 0 to 13.6 GHz, which primarily spreads around the pump laser and corresponding sidebands generated by the mechanical mode m_3, leading to three subcombs centered around frequencies of 0, 5.3, 10.6 GHz. In practice, at least seven subcombs around the pump light can be observed in our system through the optical spectrum (see Supplemental Material [48]). Furthermore, these three subcombs are, respectively, widened and intersected.

With changing the detuning, the SP is excited and its frequency ω_{sp} is around $\omega_2/3$, which results in a fraction frequency locked coherent coupling between mechanical mode m_2 and induces the appearance of additional comblines in the OMFCs, as shown in Fig. 2(b). Therefore, the OMFCs evolves to a denser comb with repetition rate $\omega_2/3$ and over 200 comblines in the RSA, which is limited by the balance between the intracavity power and SP state. Additionally, the frequency of the SP can be changed by controlling the pump detuning and switched to exact fractions of another mechanical mode m_1, as shown in Fig. 2(c). In this OMFC, the lasing state is switched to mechanical mode m_1 while maintaining the oscillation lasing state of mechaincal mode m_3, resulting in a repetition rate of $\omega_1/2$. Over 260 comblines are obtained in RSA. The corresponding oscillations in time domain for these three states are shown in Figs. 2(g)–2(i). The dynamics of this state generation and evolution are recorded and discussed in the following section.

Mode competition and multimode phonon lasing.—Figure 3(a) shows the power transmission of mechanical modes m_1, m_2 and m_3 when the pump laser is gradually scanned into the resonance before exciting the SP. It can be clearly observed that the mechanical modes m_3 first enter into the lasing state when λ_{pump} is around 1532.78 nm. Then, when λ_{pump} is around 1532.95 nm, while the mechanical mode m_3 is still in the lasing state, the

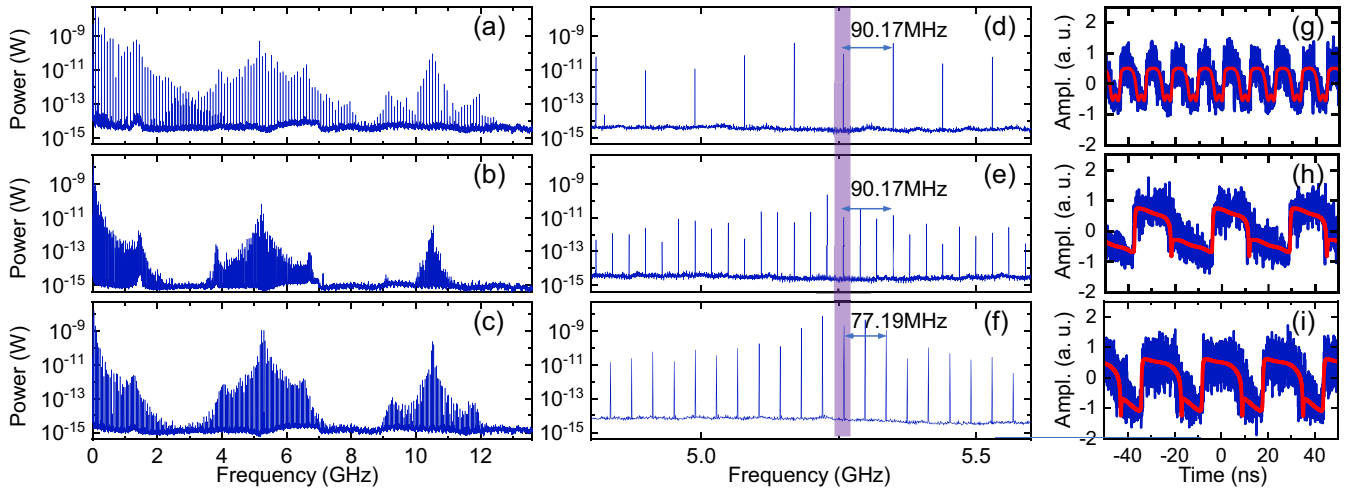

FIG. 2. The typical OMFCs. (a) The power spectrum of OMFCs with repetition rate ω_2, which consists of the multimode phonon lasing state of mechanical modes m_2 and m_3 but without the SP. (b)–(c) The power spectrum of OMFCs with repetition rate $\omega_2/3$ or $\omega_1/2$ due to the SP process. (d)–(f) The enlarged images of three typical OMFCs near ω_3 in (a)–(c). The purple shaded area represents the combline with the frequency of ω_3. (g)–(i) Corresponding time domain oscillations of OMFCs in (a)–(c). The red lines are the theoretical fitting of the pulse envelope.

mechanical modes m_1 and m_2 both start to be optomechanically gained, depicted as an increase in amplitude. However, at $\lambda_{\mathrm{pump}} = 1533$ nm, only the mechanical mode m_2 takes place lasing, meanwhile, the amplitude of mechanical mode m_1 sharply decays to zero. In short, the mechanical modes m_1 and m_2 behave as a mode competition while the mechanical modes m_2 and m_3 show a two-mode oscillation lasing, which is consistent with the previous observation.

When a mechanical mode modulates the optical field to form a frequency comb, the optical field can also modify the linewidth of the mechanical mode m_j to $\gamma_j' = \gamma_j - \chi_j$, where $j = 1, 2, 3$ and $\chi_j = \mathrm{Im}(g_j a^\dagger a/m_j)$ is the energy gain of mechanical mode m_j from the optical pump. When $\gamma_j' \le 0$, the energy gain of mechanical mode m_j exceeds its damping rate, and this mechanical mode starts lasing. Without loss of generality, we consider the energy gain of m_1:

$$\chi_1(\xi_1,\xi_2,\xi_3) = \sum_{k,p,q=-\infty}^{\infty} \mathrm{Im}\left[\frac{2g_1^2\kappa_e\kappa\varepsilon_p^2}{\kappa/2 + i(\Theta+\omega_1)} \times \frac{J_{k-1}(\xi_1)J_k(\xi_1)J_p^2(\xi_2)J_q^2(\xi_3)}{\xi_1(\kappa/2 - i\Theta)}\right], \quad (1)$$

where $\xi_j = 2g_jM_j/\omega_j$ is the normalized amplitude of each mechanical mode, with $M_j = m_j e^{i(\omega_j t+\pi/2)}$, $\Theta = \Delta - k\omega_1 - p\omega_2 - q\omega_3$, detuning between pump and cavity $\Delta = \omega_d - \omega_o$, and only coherence part of the optical pump is considered, because of the narrow linewidths of the mechanical modes. Under weak excitation of mechanical modes m_2 and m_3, i. e., $\xi_2, \xi_3 \ll 1$, terms where $p = q = 0$ play a dominant role. Here, excitation of the other mechanical mode (ξ_2 or ξ_3) reduces the energy gain of m_1, which proportional to the decreasing function $J_0^2(\xi_2)J_0^2(\xi_3)$. This mechanism underlies the mode competition in phonon lasing with which, for MPL to occur, two conditions need to be met: (i) There is a point in ξ_1, ξ_2, ξ_3 space where $\gamma_1'(\xi_1,\xi_2,\xi_3) = \gamma_2'(\xi_1,\xi_2,\xi_3) = \gamma_3'(\xi_1,\xi_2,\xi_3) = 0$. This condition means thresholds of these modes can be achieved simultaneously. (ii) Around the point above, there is $[\partial\gamma_p'(\xi_1,\xi_2,\xi_3)/\partial\xi_p][\partial\gamma_q'(\xi_1,\xi_2,\xi_3)/\partial\xi_q] > [\partial\gamma_p'(\xi_1,\xi_2,\xi_3)/\partial\xi_q][\partial\gamma_q'(\xi_1,\xi_2,\xi_3)/\partial\xi_p]$ for any $p \ne q$. This condition means that the slight deviations from the equilibrium point need to be pulled back. In previous studies [41], only the first several terms in Eq. (1) contribute to γ_j', preventing the fulfillment of condition (ii). Thus no mutimode phonon lasing occurs without external modulation. Since $\omega_3 \gg \omega_1, \omega_2$, the detuning around ω_1 is significantly large for mode m_1, m_2 and terms involving $\Delta = k\omega_1 + p\omega_2$ determine the form of function γ_j', which makes the multimode oscillation lasing state of mechanical modes m_3 and m_2 (or m_1) realizable. Figures 3(b) and 3(c) describe the trajectories of excitation thresholds ($\gamma_j' = 0$) in the amplitude space for the systems: ξ_1 and ξ_2, ξ_2 and ξ_3, respectively. For points inside (outside) the threshold trajectory $\gamma_j' = 0$, it tends to evolve along (opposite to) the direction of the ξ_j amplitude coordinate axis. It is evident that the intersections of the threshold trajectories satisfy condition (i). However, as shown in Figs. 3(d)–3(f), condition (ii) is only fulfilled in the blue intersections. Therefore, only two-mode phonon lasing between m_2, m_3 appears in such a system. By engineering the structure of the threshold curves, more kinds of MPL can be generated in the optomechanical systems.

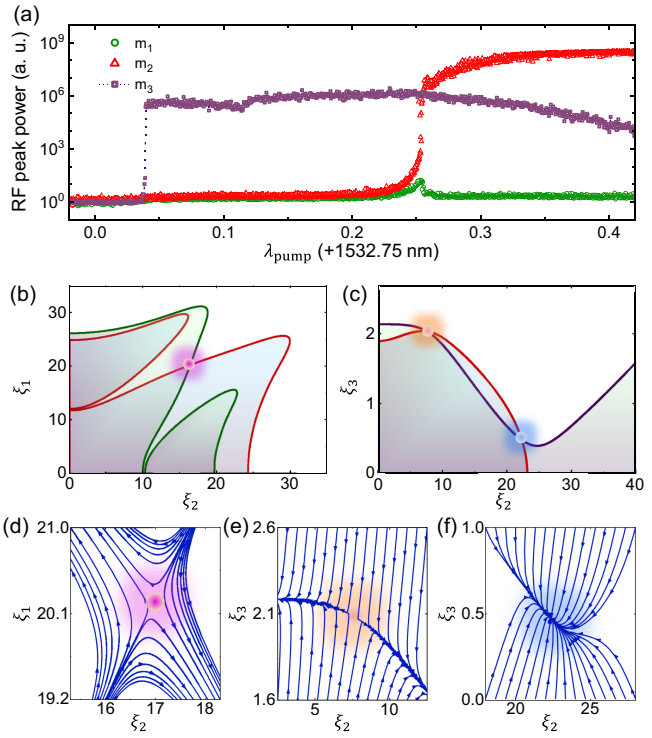

FIG. 3. The mode competition and multimode phonon lasing. (a) The power transmission of mechanical modes when scanning the pump from far-blue detuning to resonant before exciting the SP. (b)–(c) The trajectories of excitation thresholds in the amplitude space of mechanical modes m_1 and m_2 (ξ_1-ξ_2), m_2 and m_3 (ξ_2-ξ_3). For points inside (outside) the threshold trajectory, the states here tend to evolve along (opposite to) the direction of the ξ_j amplitude coordinate axis. (d)–(f) State evolution around the pink, orange, and blue crossing points of trajectories in (b)–(c).

Switching lasing state with the aid of SP.—As scanning the pump laser further towards resonance, SP is excited for the varied OMFC. Whenever $\omega_{\mathrm{SP}} = \omega_{1(2)}/N$, the optical field will be modulated to have a component with the frequency of ω_{SP}, which will provide the additional energy gain to the mechanical mode $m_{1(2)}$. Even though the energy gain caused by optomechanical coupling is already strongly suppressed by mode competition, the threshold of mode m_j could be achieved by the assistance of SP. In this scenario, the lasing state of mode m_j generally enhances the SP

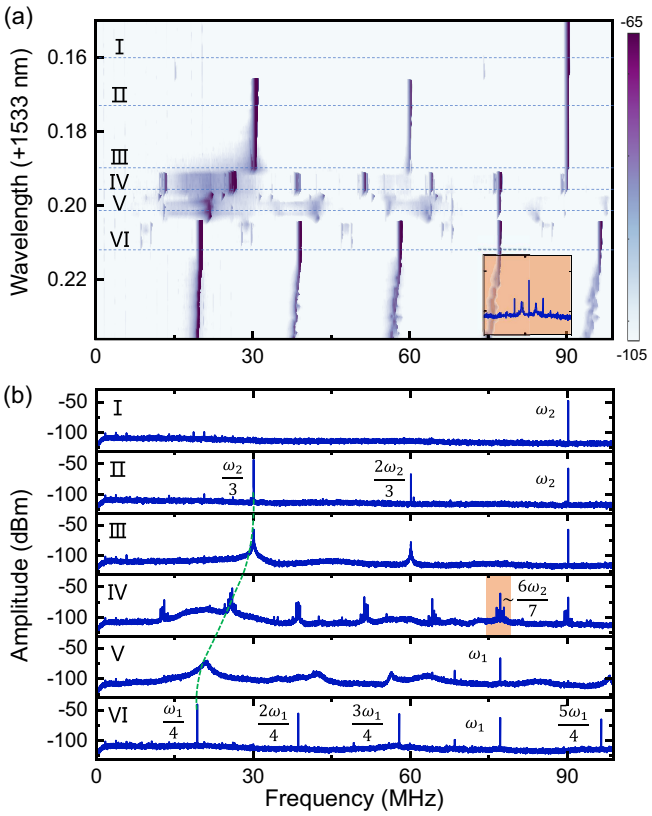

FIG. 4. Switching lasing state with the assistance of SP. (a) The dynamic evolution of the power spectrum which is continuously recorded by the RSA as scanning the pump laser further towards the resonance. The blue dashed lines I–VI indicate the different stages of dynamic evolution. (b) The typical power spectra of different stages in (a). The green dashed line illustrates the shift of the SP and interaction with the mechanical modes. Inset: enlarged image of the quasi-locked state in the orange shaded area with $\omega_{\mathrm{SP}} \approx \frac{2}{6}\omega_1 \sim \frac{2}{7}\omega_2$.

through frequency-locking effect and suppresses the lasing of other mechanical modes through mode competition, leading to a switch of the lasing state. The dynamic evolution of the lasing state is shown in Fig. 4(a). Several typical power spectra are shown in Fig. 4(b). Stage I, similar to Fig. 2(a), shows that mode m_2 is already lasing before the formation of SP. When SP is excited and ω_{SP} is approximately $\omega_2/3$, it's frequency-locked to ω_2, resulting in a coherent state with coupling between SP and mode m_2, as shown in stage II [$\sim$ Fig. 2(b)]. However, as the redshift tendency of ω_{SP} gradually deteriorates the frequency locking, the rf linewidth at $\omega_2/3$ recovers towards the wider one of pure SP (stage III). When the frequency locking becomes unsustainable, a frequency jump of ω_{SP} occurs (stage IV). Similarly, another frequency jump appears in stage V. In this case, since ω_{SP} is closer to $\omega_1/4$, energy gain caused by SP shifts towards the mode m_1, resulting in lasing in that mode. Meanwhile, the mode m_2 is suppressed by mode competition as described above.

In stage VI, SP is frequency-locked to ω_1 in a way of $\omega_{\mathrm{SP}} = \omega_1/4$, from which the state depicted in Fig. 2(c) (where $\omega_{\mathrm{SP}} = \omega_1/2$) can be achieved by scanning the λ_{pump} in reverse due to bistability of SP [52]. It is worth noting that a quasi-three-mode oscillation lasing state of mechanical modes m_1, m_2, and m_3 is observed in stage IV. It can be interpreted as SP providing intermode modulation, $\omega_{SP} = 2(\omega_2 - \omega_1)$, resembling the dynamics of Floquet modulation [42]. However, the wide linewidth of pure SP and the frequency difference ($\sim$0.09 MHz) between ω_1 and $\frac{6}{7}\omega_2$ limit the mode locking between mechanical modes m_1 and m_2, resulting in a quasi-mode-locked state, as shown in the inset of Fig. 4(a). Actually, prior to the pump exiting the optical cavity, there are additional complex evolutions that warrant further study in the future.

Conclusion.—In summary, a series of OMFCs based on multiple nonlinear dynamics is demonstrated. We experimentally and theoretically research the generations of MPLs without additional modulation, where both mechanical modes m_2 and m_3 are optically driven to self-sustained oscillation state. Additionally, by introducing SP into system, we explore a range of dynamic evolution due to the interaction among SP and flexural mechanical modes, such as frequency locking, switching of the lasing state and even a quasi-three mode oscillation lasing state of mechanical modes m_1, m_2 and m_3 with SP providing intermode quasi-Floquet modulation. The subcombs around frequency of 5.3 GHz can span over an octave as MFC. Our findings demonstrate the efficacy of utilizing multiple nonlinear dynamics in the generation and control of OMFCs. These OMFCs are expected to play an important role in the domain of sensing, timing, and metrology.

This work was supported by the National Key Research and Development Program of China (Grant No. 2020YFB2205801), Innovation program for Quantum Science and Technology (2021ZD0303203), National Natural Science Foundation of China (Grants No. 12293052, No. 12293050, No. 11934012, No. 92050109, No. 12104442, and No. 92250302), the Fundamental Research Funds for the Central Universities, the CAS Project for Young Scientists in Basic Research (YSBR-069). This work was partially carried out at the USTC Center for Micro and Nanoscale Research and Fabrication.

*These authors contributed equally to this work.
†shenzhen@ustc.edu.cn
‡chunhua@ustc.edu.cn

[1] D. J. Jones, S. A. Diddams, J. K. Ranka, A. Stentz, R. S. Windeler, J. L. Hall, and S. T. Cundiff, Carrier-envelope phase control of femtosecond mode-locked lasers and direct optical frequency synthesis, Science **288**, 635 (2000).

[2] R. Holzwarth, T. Udem, T. W. Hansch, J. C. Knight, W. J. Wadsworth, and P. S. J. Russell, Optical frequency synthesizer for precision spectroscopy, Phys. Rev. Lett. **85**, 2264 (2000).

[3] T. Udem, R. Holzwarth, and T. W. Hansch, Optical frequency metrology, Nature (London) **416**, 233 (2002).

[4] T. J. Kippenberg, A. L. Gaeta, M. Lipson, and M. L. Gorodetsky, Dissipative kerr solitons in optical microresonators, Science **361**, 567 (2018).

[5] M. Zhang, B. Buscaino, C. Wang, A. Shams-Ansari, C. Reimer, R. Zhu, J. M. Kahn, and M. Loncar, Broadband electro-optic frequency comb generation in a lithium niobate microring resonator, Nature (London) **568**, 373 (2019).

[6] C. Wang, J. Li, A. Yi, Z. Fang, L. Zhou, Z. Wang, R. Niu, Y. Chen, J. Zhang, Y. Cheng *et al.*, Soliton formation and spectral translation into visible on CMOS-compatible 4h-silicon-carbide-on-insulator platform, Light **11**, 341 (2022).

[7] Y. S. Juan and F. Y. Lin, Ultra broadband microwave frequency combs generated by an optical pulse-injected semiconductor laser, Opt. Express **17**, 18596 (2009).

[8] M. J. Hagmann, A. J. Taylor, and D. A. Yarotski, Observation of 200th harmonic with fractional linewidth of 10(-10) in a microwave frequency comb generated in a tunneling junction, Appl. Phys. Lett. **101** (2012).

[9] T. J. Kippenberg, R. Holzwarth, and S. A. Diddams, Microresonator-based optical frequency combs, Science **332**, 555 (2011).

[10] R. Niu, M. Li, S. Wan, Y. R. Sun, S.-M. Hu, C.-L. Zou, G.-C. Guo, and C.-H. Dong, khz-precision wavemeter based on reconfigurable microsoliton, Nat. Commun. **14**, 169 (2023).

[11] W. F. McGrew, X. Zhang, R. J. Fasano, S. A. Schaffer, K. Beloy, D. Nicolodi, R. C. Brown, N. Hinkley, G. Milani, M. Schioppo, T. H. Yoon, and A. D. Ludlow, Atomic clock performance enabling geodesy below the centimetre level, Nature (London) **564**, 87 (2018).

[12] M. G. Suh and K. J. Vahala, Soliton microcomb range measurement, Science **359**, 884 (2018).

[13] P. Marin-Palomo, J. N. Kemal, M. Karpov, A. Kordts, J. Pfeifle, M. H. P. Pfeiffer, P. Trocha, S. Wolf, V. Brasch, M. H. Anderson, R. Rosenberger, K. Vijayan, W. Freude, T. J. Kippenberg, and C. Koos, Microresonator-based solitons for massively parallel coherent optical communications, Nature (London) **546**, 274 (2017).

[14] E. Obrzud, M. Rainer, A. Harutyunyan, M. H. Anderson, J. Liu, M. Geiselmann, B. Chazelas, S. Kundermann, S. Lecomte, M. Cecconi, A. Ghedina, E. Molinari, F. Pepe, F. Wildi, F. Bouchy, T. J. Kippenberg, and T. Herr, A microphotonic astrocomb, Nat. Photonics **13**, 31 (2018).

[15] J. Li, X. Yi, H. Lee, S. A. Diddams, and K. J. Vahala, Electro-optical frequency division and stable microwave synthesis, Science **345**, 309 (2014).

[16] C. Reimer, M. Kues, P. Roztocki, B. Wetzel, F. Grazioso, B. E. Little, S. T. Chu, T. Johnston, Y. Bromberg, L. Caspani, D. J. Moss, and R. Morandotti, Generation of multiphoton entangled quantum states by means of integrated frequency combs, Science **351**, 1176 (2016).

[17] T. Fortier and E. Baumann, 20 years of developments in optical frequency comb technology and applications, Commun. Phys. **2**, 153 (2019).

[18] M.-G. Suh and K. Vahala, Gigahertz-repetition-rate soliton microcombs, Optica **5**, 65 (2018).

[19] Y. Hu, S. Ding, Y. Qin, J. Gu, W. Wan, M. Xiao, and X. Jiang, Generation of optical frequency comb via giant optomechanical oscillation, Phys. Rev. Lett. **127**, 134301 (2021).

[20] B. Nuss, J. Mayer, S. Marahrens, and T. Zwick, Frequency comb OFDM radar system with high range resolution and low sampling rate, IEEE Trans. Microwave Theory Techniq. **68**, 3861 (2020).

[21] S. Fukushima, C. F. C. Silva, Y. Muramoto, and A. J. Seeds, Optoelectronic millimeter-wave synthesis using an optical frequency comb generator, optically injection locked lasers, and a unitraveling-carrier photodiode, J. Lightwave Technol. **21**, 3043 (2003).

[22] T. Tokuzawa, H. Tsuchiya, T. Tsujimura, M. Emoto, H. Nakanishi, S. Inagaki, K. Ida, H. Yamada, A. Ejiri, K. Y. Watanabe, K. Oguri, T. Akiyama, K. Tanaka, I. Yamada, and L. H. D. E. Group, Microwave frequency comb Doppler reflectometer applying fast digital data acquisition system in LHD, Rev. Sci. Instrum. **89**, 10H118 (2018).

[23] M. Maldovan, Sound and heat revolutions in phononics, Nature (London) **503**, 209 (2013).

[24] M. Aspelmeyer, T. J. Kippenberg, and F. Marquardt, Cavity optomechanics, Rev. Mod. Phys. **86**, 1391 (2014).

[25] Z. Shen, Y.-L. Zhang, Y. Chen, C.-L. Zou, Y.-F. Xiao, X.-B. Zou, F.-W. Sun, G.-C. Guo, and C.-H. Dong, Experimental realization of optomechanically induced non-reciprocity, Nat. Photonics **10**, 657 (2016).

[26] J. Guo and S. Gröblacher, Integrated optical-readout of a high-q mechanical out-of-plane mode, Light **11**, 282 (2022).

[27] S.-J. Tang, M. Zhang, J. Sun, J.-W. Meng, X. Xiong, Q. Gong, D. Jin, Q.-F. Yang, and Y.-F. Xiao, Single-particle photoacoustic vibrational spectroscopy using optical microresonators, Nat. Photonics **17**, 951 (2023).

[28] Y. Wang, Z.-P. Shi, H.-Y. Kuang, X. Xi, S. Wan, Z. Shen, P.-Y. Wang, G.-T. Xu, X. Sun, C.-L. Zou, G.-C. Guo, and C.-H. Dong, Realization of quantum ground state in an optomechanical crystal cavity, Sci. China Phys. Mech. Astron. **66**, 124213 (2023).

[29] X. Liu, J. Hu, Z.-F. Li, X. Li, P.-Y. Li, P.-J. Liang, Z.-Q. Zhou, C.-F. Li, and G.-C. Guo, Heralded entanglement distribution between two absorptive quantum memories, Nature (London) **594**, 41 (2021).

[30] Z. Shen, G. T. Xu, M. Zhang, Y. L. Zhang, Y. Wang, C. Z. Chai, C. L. Zou, G. C. Guo, and C. H. Dong, Coherent coupling between phonons, magnons, and photons, Phys. Rev. Lett. **129**, 243601 (2022).

[31] M. Mirhosseini, A. Sipahigil, M. Kalaee, and O. Painter, Superconducting qubit to optical photon transduction, Nature (London) **588**, 599 (2020).

[32] G. Chen, *Nanoscale Energy Transport and Conversion: A Parallel Treatment of Electrons, Molecules, Phonons, and Photons* (Oxford University Press, New York, 2005).

[33] M. A. Miri, G. D'Aguanno, and A. Alu, Optomechanical frequency combs, New J. Phys. **20** (2018).

[34] A. Ganesan, C. Do, and A. Seshia, Phononic frequency comb via intrinsic three-wave mixing, Phys. Rev. Lett. **118**, 033903 (2017).

[35] J. Zhang, B. Peng, S. Kim, F. Monifi, X. Jiang, Y. Li, P. Yu, L. Liu, Y. X. Liu, A. Alu, and L. Yang, Optomechanical dissipative solitons, Nature (London) **600**, 75 (2021).
[36] M. H. de Jong, A. Ganesan, A. Cupertino, and R. A. Norte, Mechanical overtone frequency combs, Nat. Commun. **14**, 1458 (2023).
[37] S. Wu, Y. Liu, Q. Liu, S. P. Wang, Z. Chen, and T. Li, Hybridized frequency combs in multimode cavity electromechanical system, Phys. Rev. Lett. **128**, 153901 (2022).
[38] D. C. Mattis, *Many-Body Problem, The: An Encyclopedia of Exactly Solved Models in One Dimension (3rd Printing With Revisions And Corrections)* (World Scientific, Singapore, 1993).
[39] A. L. Gaeta, M. Lipson, and T. J. Kippenberg, Photonic-chip-based frequency combs, Nat. Photonics **13**, 158 (2019).
[40] R. C. Ng, P. Nizet, D. Navarro-Urrios, G. Arregui, M. Albrechtsen, P. D. García, S. Stobbe, C. M. Sotomayor-Torres, and G. Madiot, Intermodulation of optical frequency combs in a multimode optomechanical system, Phys. Rev. Res. **5**, L032028 (2023).
[41] U. Kemiktarak, M. Durand, M. Metcalfe, and J. Lawall, Mode competition and anomalous cooling in a multimode phonon laser, Phys. Rev. Lett. **113**, 030802 (2014).
[42] L. Mercade, K. Pelka, R. Burgwal, A. Xuereb, A. Martinez, and E. Verhagen, Floquet phonon lasing in multimode optomechanical systems, Phys. Rev. Lett. **127**, 073601 (2021).
[43] P. Barclay, K. Srinivasan, and O. Painter, Nonlinear response of silicon photonic crystal microresonators excited via an integrated waveguide and fiber taper, Opt. Express **13**, 801 (2005).
[44] J. H. Yang, T. Y. Gu, J. J. Zheng, M. B. Yu, G. Q. Lo, D. L. Kwong, and C. W. Wong, Radio frequency regenerative oscillations in monolithic high-Q/V heterostructured photonic crystal cavities, Appl. Phys. Lett. **104** (2014).
[45] M. L. Gorodetsky, A. Schliesser, G. Anetsberger, S. Deleglise, and T. J. Kippenberg, Determination of the vacuum optomechanical coupling rate using frequency noise calibration, Opt. Express **18**, 23236 (2010).
[46] S. Weis, R. Riviere, S. Deleglise, E. Gavartin, O. Arcizet, A. Schliesser, and T. J. Kippenberg, Optomechanically induced transparency, Science **330**, 1520 (2010).
[47] C. Dong, V. Fiore, M. C. Kuzyk, and H. Wang, Optomechanical dark mode, Science **338**, 1609 (2012).
[48] See Supplemental Materials at http://link.aps.org/supplemental/10.1103/PhysRevLett.132.163603 for additional information about the experimental methods and a detailed discussion of the theoretical analysis, which includes Refs. [48–50].
[49] W. E. Lamb Jr, Theory of an optical maser, Phys. Rev. **134**, A1429 (1964).
[50] G. S. MacCabe, H. Ren, J. Luo, J. D. Cohen, H. Zhou, A. Sipahigil, M. Mirhosseini, and O. Painter, Nano-acoustic resonator with ultralong phonon lifetime, Science **370**, 840 (2020).
[51] A. H. Safavi-Naeini, T. P. Mayer Alegre, J. Chan, M. Eichenfield, M. Winger, Q. Lin, J. T. Hill, D. E. Chang, and O. Painter, Electromagnetically induced transparency and slow light with optomechanics, Nature (London) **472**, 69 (2011).
[52] D. Navarro-Urrios, N. E. Capuj, M. F. Colombano, P. D. Garcia, M. Sledzinska, F. Alzina, A. Griol, A. Martinez, and C. M. Sotomayor-Torres, Nonlinear dynamics and chaos in an optomechanical beam, Nat. Commun. **8**, 14965 (2017).

Correction: The citation of a related work was missing from the published article and has been inserted as Ref. [40]. Subsequent references have been renumbered.